Journal of
Medicinal Chemistry

Article

Discovery and Optimization of Glucose Uptake Inhibitors

Kevin G. Liu, Ji-In Kim, Kellen Olszewski, Anthony M Barsotti, Koi Morris, Christophe Lamarque, Xuemei Yu, Jack Gaffney, Xiao-Jiang Feng, Jeegar Patel, and Masha Poyurovsky

J. Med. Chem., **Just Accepted Manuscript** • DOI: 10.1021/acs.jmedchem.9b02153 • Publication Date (Web): 13 Apr 2020

Just Accepted

is published by the American Chemical Society. 1155 Sixteenth Street N.W., Washington, DC 20036

Discovery and Optimization of Glucose Uptake Inhibitors

Kevin G. Liu,* Ji-In Kim, Kellen Olszewski, Anthony M. Barsotti†, Koi Morris, Christophe Lamarque, Xuemei Yu, Jack Gaffney, Xiao-Jiang Feng, Jeegar P. Patel, and Masha V. Poyurovsky

Kadmon Corporation, LLC., 450 East 29th Street, New York, NY 10016, USA. †Current address: Inzen Therapeutics, Inc., 430 East 29th Street, New York, NY 10016, USA

GLUT, GLUT1, GLUT3, glucose transport inhibitor, glucose transport, immunometabolism, inflammation

ABSTRACT: Aerobic glycolysis, originally identified by Warburg as a hallmark of cancer, has recently been implicated in immune cell activation and growth. Glucose, the starting material for glycolysis, is transported through the cellular membrane by a family of glucose transporters (GLUTs). Therefore, targeting glucose transporters to regulate aerobic glycolysis is an attractive approach to identify potential therapeutic agents for cancers and autoimmune diseases. Herein, we describe the discovery and optimization of a class of potent, orally available inhibitors of glucose transporters, targeting both GLUT1 and GLUT3.

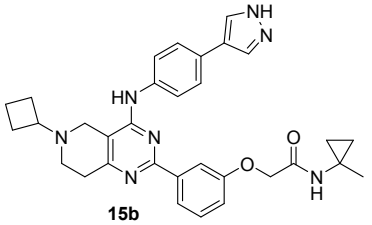

15b

GLUT1 IC_{50} = 242 nM
GLUT3 IC_{50} = 179 nM
Oral *F* = 45.5% (mouse) and 49.4% (rat)

INTRODUCTION

Glucose is the most abundant energy source for cells in human tissues. Under aerobic conditions, cells normally metabolize glucose into pyruvate in the cytosol, which is oxidized in the tricarboxylic acid (TCA) cycle to drive oxidative phosphorylation (OXPHOS) in the mitochondria. When oxygen is lacking, a condition called hypoxia, cells are forced to switch to anaerobic glycolysis where the aerobic glycolysis product pyruvate is instead converted to lactate. Glycolysis is significantly less efficient than the OXPHOS pathway, producing an order of magnitude less ATP per glucose. Despite this, both cultured cancer cells and tumors typically ferment glucose to lactate at a high rate even in the presence of abundant oxygen. This altered metabolism phenomenon, known as the Warburg effect,[1, 2] is a hallmark of cancer cells. This phenomenon which has been exploited for cancer imaging and diagnosis with the PET ligand [^{18}F]fluoro-2-deoxyglucose (^{18}F-FDG), a metabolically stable glucose analogue. There is still considerable academic debate about the nature of the survival benefit aerobic glycolysis phenomenon provides for cancer and other rapidly proliferating cells. It is, however, undisputed that elevation in the rate of glycolysis and increased glucose uptake,[3] are associated with tumor growth and present an interesting targets for potential therapeutic intervention[4-6].

Elevated rates of glucose consumption and glycolysis were recently implicated in immune cell activation and growth. Immunometabolism,[7, 8] an emerging field studying the interplay between the immune system and metabolism, has attracted considerable attention both for understanding the phenomenon and searching for new treatments for autoimmune diseases. Upon activation, naïve $CD4^+$ T cells rapidly grow, proliferate, and differentiate into functional subsets including T helper (Th) cells such as effector Th1, Th2, and Th17 cells which drive the immune response, and $Foxp3^+$ regulatory T (Treg) cells which suppress the immune activity. Unlike their precursor naïve $CD4^+$ T cells which rely predominantly on OXPHOS, effector $CD4^+$ T cells primarily rely on aerobic glycolysis for their metabolic needs and immune functions.[9, 10]

Glucose transporters (GLUTs) constitute a family of proteins that facilitate the transport of glucose across cellular membranes. To date, 14 human GLUT members (GLUT1-14) have been identified.[11] GLUTs have 12 transmembrane domains, and several crystal structures including human GLUT1 and GLUT3 have been obtained.[12, 13] Given that glucose transport is one of the rate-limiting steps in glucose metabolism, GLUTs,

especially GLUT1, are overexpressed in cancer and activated immune cells to meet their glucose demands, and have become an interesting therapeutic target for cancers and autoimmune diseases.[9, 10, 14-16]

A number of GLUT (mainly GLUT1) inhibitors have been reported. Representative GLUT inhibitors are summarized in Chart 1. Compounds **1-3** [17-19] have limited potency (in the μM to mM range) and have been reported to have additional activity independent of GLUT inhibition. Compound **4** of peptidic nature and its analogue have been reported as GLUT inhibitors and co-crystallized with hGLUT1.[20] Compounds **5**[21] and **6** (BAY-876)[22], reported by Siebeneicher and co-workers at Bayer, represent two classes of GLUT1 sub-type selective inhibitors. Compound **6** was reported to be a potent and orally bioavailable GLUT1 selective inhibitor. Very recently, Waldmann et al., disclosed a potent GLUT1/2/3 inhibitor **7** (Glutor) and its ability to suppress growth of a number of cancer cell lines. However, no pharmacokinetic or *in vivo* functional data associated with this compound was disclosed.[23]

Chart 1. Known GLUT inhibitors

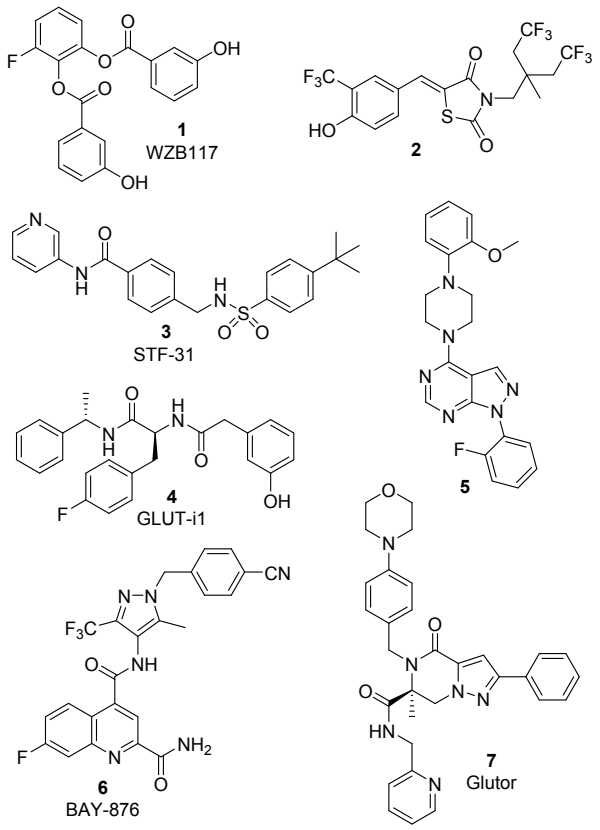

As part of our research efforts in metabolomics, we were interested in studying the inhibition of glucose uptake and its potential therapeutic indications. While a number of above-mentioned compounds have been tested in cell-based assays, little or no *in vivo* functional data is available. This is due in part to their poor pharmacokinetic properties which limit the ability to fully interrogate the potential therapeutic utility of GLUT inhibitors. In order to assess the clinical potential of GLUT targeting, we set out to generate GLUT inhibitors with optimized safety and PK profiles. To avoid possible compensatory mechanisms from GLUT3 following GLUT1 inhibition, we additionally aimed to generate compounds targeting both isoforms.

RESULTS AND DISCUSSION

Dihydrofuropyrimidine and dihydropyranopyrimidine derivatives. To identify novel glucose uptake inhibitors, we screened Kadmon's compound collection utilizing a high-throughput cell-based phenotypic assay. In this assay, HT-1080 colorectal cancer cells were treated with 10 μM oligomycin to inhibit ATP synthase, blocking mitochondria-derived ATP production through oxidative phosphorylation and rendering the cells dependent on glycolytic ATP production. Glycolytically-derived ATP production was measured with the Cell Titer-Glo™ assay kit (Promega). HT-1080 cells express both GLUT1 and GLUT3 transporters, so the inhibitory activity of our compounds in these cells is referred to broadly as "GLUT" inhibition. Because simply inhibiting ATP production cannot be linked to inhibition of glucose uptake directly, we confirmed inhibition of glucose transport, but not other targets such as downstream glycolysis enzymes, by also measuring direct glucose uptake, lactate secretion, glutamine consumption and metabolomic profiling of treated cells. The results from the above-mentioned experiments supported the direct blockade of glucose transport mechanism and were further reinforced by the *in vivo* glucose tolerance and imaging experiments (Olszewski, et al., manuscript in preparation). GLUT subtype activity was measured using cell lines that specifically express the GLUT isoforms, e.g., GLUT1 (DLD1); GLUT3 (DLD1-*SLC2A1*$^{-/-}$). We initially utilized the GLUT assay in HT1080 cells to identify hits and lead chemical series. As the project progressed, we relied primarily on more informative GLUT1 and GLUT3 subtype assays for lead optimization.

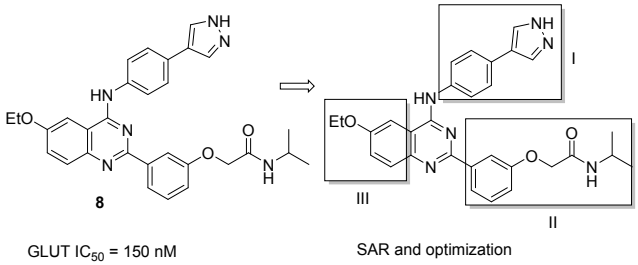

Figure 1. The screening hit and optimization strategy

Our screening efforts led to the identification of compound **8** (Figure 1) as a potent GLUT inhibitor (IC_{50} = 150 nM). To elucidate the molecular mechanism of GLUT inhibition we compared the activity of compound **8** in a GLUT1 inhibition assay to cytochalasin B at varying glucose concentrations. Cytochalasin B has been extensively characterized as a glucose competitive inhibitor of GLUT1, which functions by binding in the glucose pocket in the central cavity of the transporter.[20, 24] We observed that both cytochalasin B and compound **8** exhibited a similar level of competition with glucose, with the GLUT1 IC_{50} for compound **8** shifting from 268 nM at 10 mM glucose to 33 nM in the presence of 0.37 mM glucose (Figure 2 and Supplementary Table S1). These

data suggested that the molecular mechanism of inhibition of glucose import by our compounds was through direct competition for the glucose binding pocket of GLUT1.

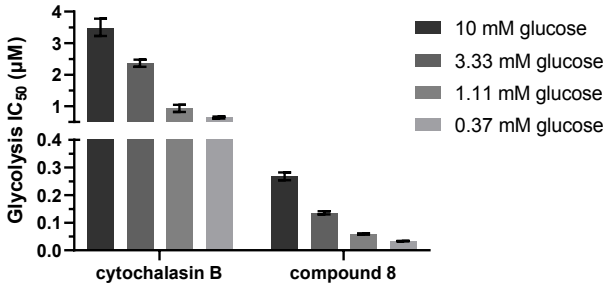

Figure 2. Compound **8** is competitive with glucose. GLUT1 IC_{50} values for cytochalasin B and compound **8** at different glucose concentrations. Graph shows calculated IC_{50} values +/- the 95% confidence interval.

While being a potent hit as a starting point, this compound was characterized by suboptimal physicochemical properties, such as poor aqueous solubility (3.36 μM, 0.01 μM, 0.03 μM at pH 2.0, pH 4.5, and pH 6.8, respectively), high protein binding (>99.9%), and poor permeability (Caco-2 P_{app} 2.0×10^{-6} cm/s). To follow up on compound **8**, we studied the SAR (structure-activity relationship) and carried out optimization in three regions of the molecule: phenylpyrazole region I, phenoxylacetamide II, and quinazoline core III (Figure 2). For region I, we replaced phenylpyrazole with a variety of groups such as small monocyclic rings, fused rings, and those that are structurally similar to phenylpyrazole. Disappointingly, all the replacements resulted in either a complete loss or a dramatic reduction of GLUT activity. Phenylpyrazole was strongly preferred in this region. It is worth mentioning that the high preference for phenylpyrazole in this region was maintained with concomitantchange to other portions of the molecules.

Aiming to improve the physicochemical properties and to enhance drug-like properties, we undertook further optimization of region II. We first removed the phenyl ring in order to reduce the total number of aromatic rings[25] or replace the phenyl ring with a saturated ring system in order to reduce sp^2 and to increase sp^3 hybridization characteristics of the molecule aiming to improve the physico-chemical property[26] as well as to potentially improve the potency by incorporating moieties similar to the glucose ring.[26] Unfortunately, these efforts were not successful as the phenyl group was shown to be required for GLUT activity. Replacement of the phenyl ring by heterocycles also led to inactivity. We then kept the phenyl group, but replaced the amide moiety with non-amide groups such as acyclic amine or ether, lactams, heterocycles or heteroaryls with the hope that these groups can avoid the potential metabolic liability of the amide group. Once again, these replacements resulted in significantly reduced potency (> 5 μM).

Upon further optimization, we found that the quinazoline core (region III) tolerated modifications without loss of GLUT activity. Although replacement of the quinazoline core with pyrimidine or substituted pyrimidines resulted in dramatic loss of activity, fusing the pyrimidine ring with a variety of heterocycles provided alternatives to the quinazoline ring which retained potency. Some of the explored heterocycle-fused pyrimidine cores are summarized in Table 1.

Table 1. Select heterocycle-fused pyrimidine cores[a]

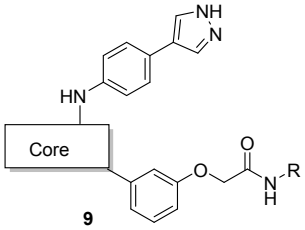

9

Entry	Core	GLUT IC_{50} (nM)	Entry	Core	GLUT IC_{50} (nM)
8	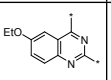	150	**9a**		200
9b		259	**9c**	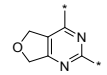	74
9d		328	**9e**		146
9f		3474	**9g**		36
9h	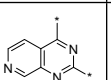	38	**9i**		350
9j	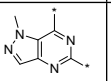	1980	**9k**		298
9l	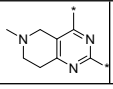	282	**9m**	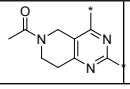	110

[a] IC_{50} values are average of at least two determinations.

While most of the compounds with heterocyle-fused pyrimidine cores (**9a-m**) are expected to have improved physical properties over quinazoline derivative **8** by simply having reduced cLogP with the introduction of additional heteroatoms, compounds **9c** and **9l** were more interesting to us due to their increased sp^3 hybridization feature contributed by the dihydrofurano- and tetrahydropyrido- groups, respectively. The increased sp^3 content was expected to translate into less molecular flatness and enhanced water solubility.

Select SAR of dihydrofuropyrimidine and dihydropyranopyrimidine derivatives is summarized Table 2. The data clearly shows that the amide N-H is required for both GLUT1 and GLUT3 activity as *N,N*-disubstituted amides (**10e** and **10f**) are either significantly less active or inactive. The most potent dihydrofuropyrimidine derivative identified, **10g,** displayed an IC_{50} of 37 nM and 12 nM against GLUT1 and GLUT3, respectively. BAY-876 (**6**) was also tested in our

assays and was shown to be a potent GLUT1 selective inhibitor as reported.[22]

The SAR of 6-membered ring dihydropyranopyrimidine derivatives in general was consistent to that of their 5-membered ring dihydrofuranopyrimidine analogues. Two of the most potent compounds identified are **11a** and **11b** (Table 2).

Table 2. SAR of dihydrofuranyl and dihydropyranyl derivatives[a]

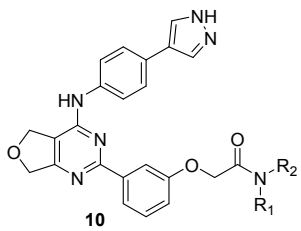

10

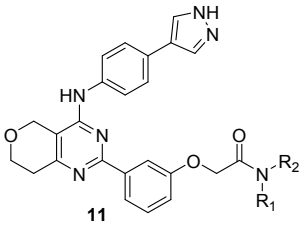

11

Entry	R1	R2	GLUT1 IC_{50} (nM)	GLUT3 IC_{50} (nM)
10a	H	*n*Pr	447	298
10b	H	*c*Pr	666	238
9c	H	*i*Pr	289	97
10c	H	*c*Bu	179	68
10d	H	*c*Pe	102	47
10e	Et	Et	1828	686
10f	-$(CH_2)_4$-		>10000	1414
10g	H	*t*Pe	37	12
10h	H	CF_3CH_2	565	160
10i	H	Ph	885	325
11a	H	3-Pe	48	33
11b	H	*t*Bu	36	26
6	---	---	50 (2[b])	4809 (1670[b])

[a]IC_{50} values are average of at least two determinations. [b]Reported data in reference [22].

The *in vitro* ADME and *in vivo* PK profiles of **10g** and **11a** are summarized in Table 3. Compound **10g** was characterized by very poor water solubility at pH 6.8 and pH 4.5 while it was more soluble at lower pH (2.0) due to its basicity. Compound **10g** was also characterized by a relatively low mouse liver microsomal stability (29 min), modestly high protein binding (f_u = 3%), and good plasma stability. The 6-membered ring dihydropyranopyrimidine derivative **11a** was more soluble, displaying solubility of 32 μM, 0.75 μM, and 0.19 μM at pH 2.0, pH 4.5, pH 6.8, respectively. The increased solubility of **11a** is presumably due to the higher degree of flexibility of dihydropyranyl and 3-pentyl groups present in **11a** as compared to their corresponding groups in **10g (Table 3)**.

In the *in vivo* mouse PK studies, both **10g** and **11a** were orally bioavailable. The relatively low oral bioavailability (22% and 28% for **10g** and **11a**, respectively) may be due in part to their relatively high intrinsic clearance and poor water solubility. Both compounds are characterized by a modest volume of distribution (1.42 and 0.63 L/kg for **10g** and **11a**, respectively). The lower volume of distribution of **11a** may have been due to its higher plasma protein binding that helped confine the drug in the plasma.

Table 3. ADME and PK profile of **10g** and **11a**[a]

Compound		**10g**	**11a**
Solubility @ pH 2.0/4.5/6.8 (μM)[b]		5.9/0.08/0.03	32/0.75/0.19
mLM stability ($t_{1/2}$, min)[c]		29	29
mPPB (%)[d]		97.0	99.7
Mouse plasma stability[e]		>95%	>95%
Mouse PK[f]	Oral Cmax (ng/mL)	1233	1870
	Oral AUC (ng/mL)	3299	5982
	CL (mL/min/kg)	34.0	23.2
	V_{dss} (L/kg)	1.42	0.63
	$t_{1/2}$ (h)	2.94	0.92
	F (%)	22	28
	B/P[g]	0.15	0.10

[a]The *in vitro* ADME data are average values of at least two determinations; The *in vivo* PK parameters are average values from three animals. [b]Solubility was determined in PBS buffer solutions. [c]Mouse liver microsomal $t_{1/2}$: 2 μM substrate, 0.5 mg/mL pooled liver microsomes, 1 mM NAPDH, 37 °C. [d]Mouse plasma protein binding. [e]Percentage of compound remaining after 18 h. [f]iv dose 10 mg/kg, vehicle 10% DMSO/40% PEG400/50% water; po dose 30 mg/kg, vehicle 0.5% methylcellulose/0.25% Tween-80 in water. [g]Compound brain and plasma exposure ratio measured at 2 h following oral administration.

Unlike other organs, brain is uniquely dependent on glucose for survival and function. To avoid potential toxicities associated with the blockade of neuronal glucose uptake we aimed to keep compound brain exposure levels to a minimum. Similar to Lipinski's landmark rule of 5 (Ro5) for drug oral bioavailability,[27] desirable physicochemical properties for brain penetration have been extensively studied using successful CNS drugs and drug candidates.[28-31] The GLUT inhibitors like **10g** and **11a** fall well outside of the CNS preferred range as they are characterized by high molecular weight (~500 Da), high *t*PSA (>100 Å^2), and high number of hydrogen bond donors (HBDs, 3) and therefore were not expected to exhibit significant brain penetration. As predicted, **10g** and **11a** were found to be only modestly brain penetrant with measured *in vivo* brain and plasma ratios of 0.15 and 0.10, respectively.

While being potent and orally bioavailable, **10g** and **11a** still possessed some undesirable physical properties such as poor water solubility. We therefore focused our efforts on other classes of compounds with improved physicochemical properties.

Tetrahydropyridopyrimidine derivatives. To identify compounds with improved aqueous solubility, we turned our attention to the tetrahydropyridopyrimidine derivatives represented by **9l** (Table 1). The pKa value of the piperidinyl nitrogen of **9l** is expected to be ~10. Under physiological pH (7.4), it should be mostly protonated, increasing the overall compound aqueous solubility.

The SAR of select tetrahydropyridopyrimidine derivatives is summarized in Table 4. Several substituents including H, Me, Et and *i*Pr on the piperidinyl nitrogen (R^1) and a number of groups on the amide nitrogen were explored. In general, this class of compounds are dual GLUT1 and GLUT3 inhibitors. Relatively bulkier amide groups (R^2) such as *t*Pe and *t*Bu (e.g. **12e, 12f, 12j, 12p**) tended to be associated with increased GLUT1 and GLUT3 activity and retained glucose competitive MOA (supplementary table S1), while relatively smaller groups such as *i*Pr (**9l**, **12g**, **12k**, **12m**) provided compounds with reduced GLUT1 potency. Among these analogues, **12p** displayed an overall more favorable pharmacological and pharmaceutical profile. The ADME and pharmacokinetic data of **12p** are summarized in Table 5.

Table 4. SAR of tetrahydropyridopyrimidine derivatives[a]

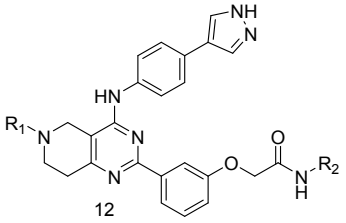

12

cpd	R1	R2	GLUT1 IC_{50} (nM)	GLUT3 IC_{50} (nM)
9l	Me	*i*Pr	1266	867
12a	Me	*i*Bu	---	846
12b	Me	*c*Bu	763	566
12c	Me	*c*Pe	559	391
12d	Me	3-Pe	789	584
12e	Me	*t*Bu	359	368
12f	Me	*t*Pe	342	391
12g	H	*i*Pr	1458	365
12h	H	*c*Pe	459	138
12i	H	3-Pe	441	121
12j	H	*t*Bu	220	58
12k	Et	*i*Pr	1578	846
12l	Et	*t*Bu	552	482
12m	*i*Pr	*i*Pr	2711	619
12n	*i*Pr	*i*Bu	1890	802
12o	*i*Pr	*c*Pe	1112	548
12p	*i*Pr	*t*Bu	326	412

[a]IC_{50} values are average of at least two determinations.

As expected, **12p** had dramatically increased water solubility (256 μM, 189 μM, and 47 μM at pH 2.0, 4.5, and 6.8, respectively) over dihydrofuropyrimidine or dihydropyranopyrimidine derivatives (e.g. **10g** and **11a**). This compound was also characterized by overall favorable ADME properties including good liver microsomal stability in mouse ($T_{1/2}$ 76 min) and rat ($T_{1/2}$ 64 min), low protein binding (83%, mouse), good plasma stability, and good permeability (P_{app} A-B 7.1×10^{-6} cm/s). In the mouse pharmacokinetic studies, **12p** displayed high oral bioavailability (61%), good plasma exposure levels (AUC 7745 ng/mL @ 30 mg/kg, po) and low brain penetration (B/P = 0.07). However, in rat, **12p** displayed a less favorable pharmacokinetic profile, which was characterized by low plasma exposure level (Cmax 399 ng/mL) and low oral bioavailability (20%). Relatively low rat plasma exposure for **12p** necessitated further optimization in order to identify compounds with improved PK across multiple species.

Table 5. ADME and PK profile of **12p**[a]

Solubility @ pH 2.0/4.5/6.8 (μM)[b]	256/189/47	
LM stability ($t_{1/2}$, min)[c]	76 (mouse), 64 (rat)	
mPPB (%)[d]	83	
Mouse plasma stability[e]	>95%	
Caco-2 P_{app} (10^{-6} cm/s)[f]	A-B 7.1 / B-A 12.4	
PK[g]	Mouse	Rat
Oral Cmax (ng/mL)	1418	399
Oral AUC (ng/mL)	7745	2267
CL (mL/min/kg)	40.6	44.3
V_{dss} (L/kg)	3.00	4.44
$t_{1/2}$ (h)	1.68	1.86
F (%)	61	20
B/P[h]	0.07	---

[a]The *in vitro* ADME data are average values of at least two determinations; The *in vivo* PK parameters are average values from three animals. [b]Solubility was determined in PBS buffer solutions. [c]Mouse and rat liver microsomal $t_{1/2}$: 2 μM substrate, 0.5 mg/mL pooled liver microsomes, 1 mM NAPDH, 37 °C. [d]Mouse plasma protein binding. [e]Percentage of compound remaining after 18 h. [f]Apparent permeability coefficients (P_{app}) of test compounds at 5 μM across Caco-2 cell monolayers: apical to basolateral (A-B) and basolateral to apical (B-A). [g]iv dose 10 mg/kg, vehicle 10% DMSO/40% PEG400/50% water; po dose 30 mg/kg, vehicle 0.5% methylcellulose/0.25% Tween-80 in water. [h]Compound brain and plasma exposure ratio measured at 2 h following oral administration.

Incorporation of a basic group to a molecule can in general help its water solubility, yet higher basicity may decrease its permeability as the positively charged form of the molecule resulted from protonation under physiological conditions tends to interact with negatively charged lipid membranes, thereby hindering its permeability.[32] The charged form also has reduced lipophilicity and thus limits its passive diffusion ability across the gut wall. We therefore tried to modulate the basicity of the piperidinyl nitrogen with the hope that this

kind of fine-tuning can help enhance oral bioavailability while maintaining the favorable physical properties.

Compound **13a**, a fluorinated analogue of **12p**, was then synthesized (Table 6). Fluorine has been extensively used in drug design to influence compound pKa, conformation, potency, and membrane permeability.[33, 34] A fluorine atom at the beta-position of an amine can reduce the pKa value by ~1.5 units. We postulated that the reduced basicity would translate into rat PK improvement. Indeed, as we expected, **13a** did display improved rat PK parameters (Table 7) including plasma exposure levels (Cmax 1875 ng/mL), clearance (23.5 mL/min/kg), and oral bioavailability (31%) over **12p** (Cmax 399 ng/mL, clearance 44.3 mL/min/kg, oral F 20%). Minimal food effect was observed in dog following oral administration at 10 mg/kg with 31% and 43% oral bioavailability, when fed and fasted, respectively. Compound **13a** showed robust linear rat PK profile up to 300 mg/kg dose. Unfortunately, there were also signs of toxicity at high doses in both mouse and rat. While the cause of observed toxicity was not fully elucidated, brain penetration of **13a** was found to be 0.15 (brain/plasma ratio). This level of brain penetration was not optimal for this target, and may have at least partially contributed to the observed toxicity.

Table 6. Additional tetrahydropyridopyrimidine derivatives

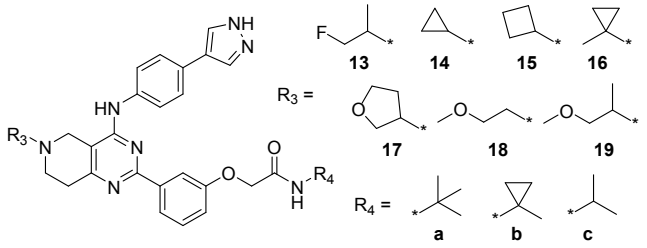

Cpd	GLUT1 IC_{50} (nM)	GLUT3 IC_{50} (nM)	Caco-2 ER[a]	B/P[b]
13a	105	232	7.33/6.23	0.15
14b	72	211	11.97/4.52	0.10
14c	140	548	10.52/5.60	0.062
15a	259	287	4.58/6.09	0.10
15b	242	179	11.19/4.33	0.050
15c	914	238	13.20/3.97	0.046
16c	1048	392	7.11/4.83	0.15
17a	161	155	4.25/3.53	0.073
18a	143	175	12.26/3.01	0.062
19a	128	275	7.20/2.94	0.064

[a]Efflux ratio calculated by $P_{app(B-A)}/P_{app(A-B)}$. [b]Compound brain and plasma exposure ratio at 1 h following oral administration at 100 mg/kg in CD-1 mice.

Table 7. ADME and PK profile of **13a**[a]

Solubility @ pH 2.0/4.5/6.8 (μM)[b]	305/212/1.1
LM stability ($t_{1/2}$, min)[c]	100 (mouse), 60 (rat)
mPPB (%)[d]	92
Mouse plasma stability[e]	>95%
Rat PK[f]	
Oral Cmax (ng/mL)	1875
Oral AUC (ng/mL)	6720
CL (mL/min/kg)	23.5
V_{dss} (L/kg)	2.01
$t_{1/2}$ (h)	1.95
F (%)	31

[a]The *in vitro* ADME data are average values of at least two determinations; The *in vivo* PK parameters are average values from three animals. [b]Solubility was determined in PBS buffer solutions. [c]Mouse and rat liver microsomal $t_{1/2}$: 2 μM substrate, 0.5 mg/mL pooled liver microsomes, 1 mM NAPDH, 37 °C. [d]Mouse plasma protein binding. [e]Percentage of compound remaining after 18 h. [f]iv dose 10 mg/kg, vehicle 10% DMSO/40% PEG400/50% water; po dose 30 mg/kg, vehicle 0.5% methylcellulose/0.25% Tween-80 in water.

Both passive diffusion and transporter-mediated processes are major mechanisms for brain permeability.[35] The brain penetration of the GLUT inhibitors reported here is likely mainly driven by passive diffusion due to their relatively high lipophilicity and lack of active transporter-recognized moieties. Several approaches were explored to lower brain penetration, such as incorporating a carboxylic acid group or significantly increasing the hydrophilicity of the molecule with the hope that the carboxylate (formed *in vivo*) or the increased molecular polarity would reduce their ability to get into the brain through the passive diffusion mechanism. However, in line with the above described SAR exploration, compounds generated through these changes either totally lost GLUT activity or were not orally bioavailable.

Xenobiotics are either blocked from entering the brain by tight junctions between brain vascular endothelial cells (BVECs) of the BBB or are rapidly pumped out from the BVECs by ATP-dependent transporter proteins such as P-glycoprotein (P-gp) and Breast Cancer Resistance Protein (BCRP). Compounds designed to act as substrates for these efflux transporters in order to lower brain penetration have been reported.[36] We tried to adapt this approach by designing and identifying compounds with efflux property as measured by *in vitro* caco-2 assay. Caco-2 cells express efflux transporters and have been widely used as a model of the intestinal or brain barrier.[37]

We then designed and synthesized a number of compounds aiming to marginally increase polarity of the molecule to facilitate efflux and to slightly reduce the basicity of piperidinyl nitrogen to help rat PK (Table 6). For the amide region, smaller and less hydrophobic groups including *i*Pr and 1-methylcyclopropyl were introduced. For the piperidinyl group, slightly electron-withdrawing groups were chosen to reduce the basicity of the nitrogen either through hyperconjugation (e.g. cyclopropyl group, **14**) or through inductive effect (e.g.

methoxyethyl, **18**). With the exception of **15c** and **16c**, these compounds maintained good GLUT1 and GLUT3 activity and when tested, **14c** and **15b** maintained glucose competitive MOA, suggesting that the binding site was retained by all the compounds across our SAR efforts (Supplementary Table S1). The efflux ratios of these compounds were in the range of approximately 1 to 4. As a result, compounds with reduced brain penetration were identified. For example, **14c**, **15b**, **15c**, **18a**, and **19a** all displayed a brain/plasma ratio below 0.07. The B/P ratios were plotted against Caco-2 efflux ratio values (Figure 3) in order to see their relationship. These data indicated that a small degree of correlation between brain penetration and Caco-2 efflux ratio exists for the compounds examined.

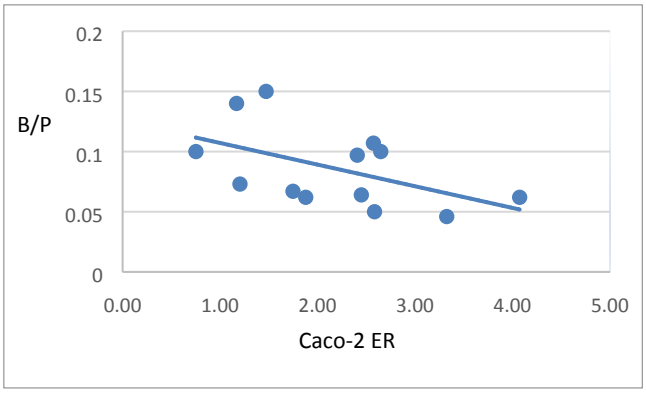

Figure 3. Plot of brain and plasma exposure ratio (B/P) at 1 h following oral administration at 100 mg/kg in CD-1 mice versus Caco-2 efflux ratio.

Most of the compounds in Table 6 displayed high plasma exposure levels in mice following oral administration (data not shown). A single 100 mg/kg dose of compounds **14c**, **15b** and **17a** was well tolerated without obvious adverse effects. Compound **15b** was chosen to be further profiled due to its overall favorable properties. The profile of **15b** is summarized in Table 8. While being very soluble at lower pH (> 200 μM at pH 2.0 and pH 4.5), **15b** displayed much lower solubility at pH 6.8 (1.4 μM). The compound is characterized by modest to good liver microsomal and plasma stability across all species. In PK studies, **15b** showed good oral bioavailability in both mouse (45.4%) and rat (49.4%) at 30 mg/kg dose. Linear PK was observed in rats up to 300 mg/kg without obvious adverse effects. In dog PK study at 10 mg/kg orally, **15b** displayed a modest food effect with a 19% (fed) and a 29% (fasted) oral bioavailability. It is worth noting that the PK studies were typically done with methylcellulose/tween-80 standard formulation for the compounds. A number of other commonly used oral formulations, e.g. cyclodextrins, were explored and it was found that 2-hydroxypropyl-β-cyclodextrin significantly enhanced oral bioavailability and plasma exposure levels of **15b**. However, with this PK-enhanced formulation, a mild and transient toxicity was observed following oral administration of **15b** at 100 mg/kg dose in mice.

Safety profiling of **15b** showed low potential for QT prolongation with an estimated IC_{50} greater than 10 μM in the manual patch clamp hERG channel assay. It also had no appreciable activity when tested at 10 μM in a safety screening panel that included 31 receptors, ion channels, and transporters.

Table 8. ADME and PK profile of **15b**[a]

Solubility @ pH 2.0/4.5/6.8 (μM)[b]	291/256/1.4	
LM stability ($t_{1/2}$, min)[c]	70 (m), 63 (r), 58 (d), 116 (h)	
PPB (%)[d]	79.8 (m), 98.9 (r), 99.0 (d), 99.3 (h)	
Mouse plasma stability[e]	>95%	
PK[f]	Mouse	Rat
Oral Cmax (ng/mL)	2525	1675
Oral AUC (ng/mL)	5890	6813
CL (mL/min/kg)	40	37
V_{dss} (L/kg)	1.70	4.51
$t_{1/2}$ (h)	0.785	2.59
F (%)	45.4	49.4
B/P[b]	0.05	---

[a]The *in vitro* ADME data are average values of at least two determinations; The *in vivo* PK parameters are average values from three animals. [b]Solubility was determined in PBS buffer solutions. [c]Mouse, rat, dog, and human liver microsomal $t_{1/2}$: 2 μM substrate, 0.5 mg/mL pooled liver microsomes, 1 mM NAPDH, 37 °C. [d]Mouse, rat, dog, and human plasma protein binding. [e]Percentage of compound remaining after 18 h. [f]iv dose 10 mg/kg, vehicle 10% DMSO/40% PEG400/50% water; po dose 30 mg/kg, vehicle 0.5% methylcellulose/0.25% Tween-80 in water.

When dosed orally, a number of compounds including **8**, **10g**, and **15b** showed *in vivo* efficacy in tumor xenograft models as well as models of autoimmune conditions at doses devoid of overt toxicity (data not shown). These data further support the notion that pharmacological blockade of glucose transport *in vivo* may have therapeutic benefits across multiple disease areas, and will be presented elsewhere.

CHEMISTRY

The synthesis of boronic esters **23** and THP protected 4-aminophenylpyrazole **26** is depicted in Scheme 1. These are necessary intermediates for the synthesis of the final compounds. The chloroacetamides **21** were easily synthesized from amines **20** and 2-chloroacetyl chloride. Alkylation of 3-bromophenol with **21** followed by Pd-mediated coupling with bis(pinacolato)diboron afforded boronic esters **23**. Alternatively, boronic esters **23** were prepared by direct alkylation of 3-(4,4,5,5-tetramethyl-1,3,2-dioxaborolan-2-yl)phenol with **21**. THP protected 4-aminophenylpyrazole **26** was synthesized in two steps from readily available **24**.

The synthesis of **8**, **9a-f**, and **9h-k** (Scheme 2) was accomplished by starting with fused 1,4-dichloropyrimidines **27** (with the fused ring designated as W) that are either commercially or synthetically available. Nucleophilic substitution with 4-(1H-pyrazol-4-yl)

aniline[38] exclusively or predominantly occurred at the 4-position of the pyrimidine ring to provide free pyrazole **28**. The free pyrazole **28** successfully went through Suzuki coupling with **23** in a microwave oven at 180 °C for 2 h to provide the final compounds in good yields. Alternatively, free pyrazole **28** was protected with Boc or THP protecting groups (**29** and **30**) and Suzuki coupling was then carried out under more conventional reaction conditions (e.g. 100 °C, overnight). These synthetic routes in general worked well for the synthesis of majority of the final compounds with a few exceptions including **9g**. Attempts to synthesize the dichloropyrimidine **27** core of **9g** failed due to its stability issue. Compound **9g** was then synthesized through a different and slightly lengthier route that is depicted in Scheme 3.

Scheme 1. Synthesis of boronic esters and THP protected 4-aminophenylpyrazole intermediates[a]

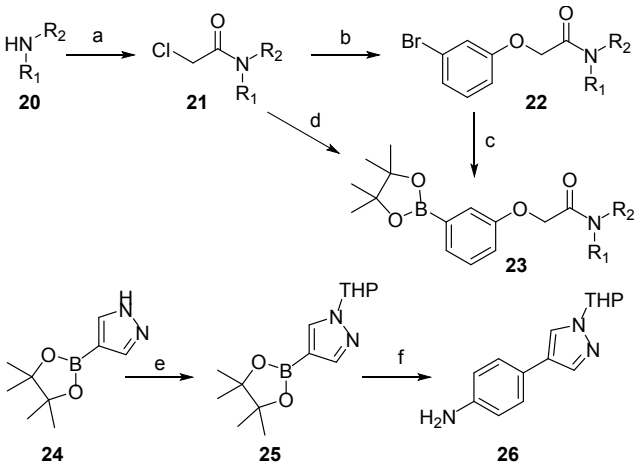

[a]Reagents and conditions: (a) 2-chloroacetyl chloride, Na_2CO_3, water, rt, 1 h; (b) 3-bromophenol, K_2CO_3, DMF, 80 °C, 12h; (c) 4,4,4',4',5,5,5',5'-octamethyl-2,2'-bi(1,3,2-dioxaborolane, $Pd(dppf)Cl_2$, AcOK, dioxane, 85 °C, 16 h; (d) 3-(4,4,5,5-tetramethyl-1,3,2-dioxaborolan-2-yl)phenol, K_2CO_3, DMF, 80 °C, 12 h; (e) DHP, *p*-TsOH, DCM, 20 °C, 4 h; (f) 4-bromoaniline, $Pd(dppf)Cl_2$, K_2CO_3, dioxane/water, 100 °C, 16 h.

One general synthesis of the tetrahydropyridopyrimidine derivatives is depicted in Scheme 4. This synthetic route allows efficient derivatization on the piperidinyl nitrogen. The synthesis started with commercially available Boc protected 1,4-dichloropyrimidine **44** followed by aromatic nucleophilic substitution, Suzuki coupling, and deprotection to provide free piperidine **47**, which was then derivatized through alkylation, reductive amination, or acylation.

Scheme 2. Synthesis of **8**, **9a-f**, **9h-k**[a]

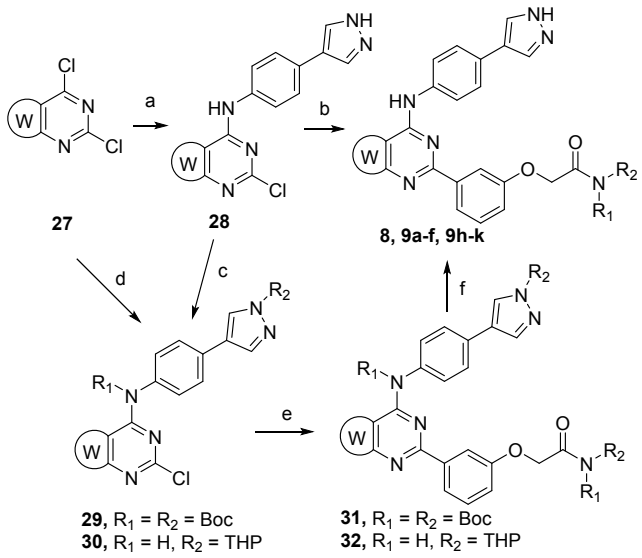

[a]Reagents and conditions: (a) 4-(1*H*-pyrazol-4-yl)aniline, *i*Pr_2NEt, DMF, 90-110 °C, 3h; (b) **23**, $Pd(PPh_3)_4$, 9:1 dioxane/water, Na_2CO_3, microwave, 180 °C, 2h; (c) Boc_2O, DMAP, TEA, DCM, 50 °C, 1.5 h; (d) *i*Pr_2NEt, *n*-BuOH, 90-110 °C, 16 h; (e) $Pd(dppf)Cl_2$, K_2CO_3, dioxane/water, 100 °C, 16 h; (f) HCl in dioxane or TFA/DCM, rt, 2 h.

Another general synthesis of the tetrahydropyridopyrimidine derivatives is depicted in Scheme 5. This general synthesis allows efficient modification of the amide region of the molecule. The synthesis started with double Michael addition of amine **48** to ethyl acrylate affording **49** followed by intramolecular Claisen condensation of **49** providing **50.** Subsequent cyclization with urea followed by chlorination provided substituted piperidine fused 1,4-dichloropyrimidine **52,** which further underwent Suzuki coupling followed by deprotection to provide the final compounds.

Scheme 3. Synthesis of **9g**[a]

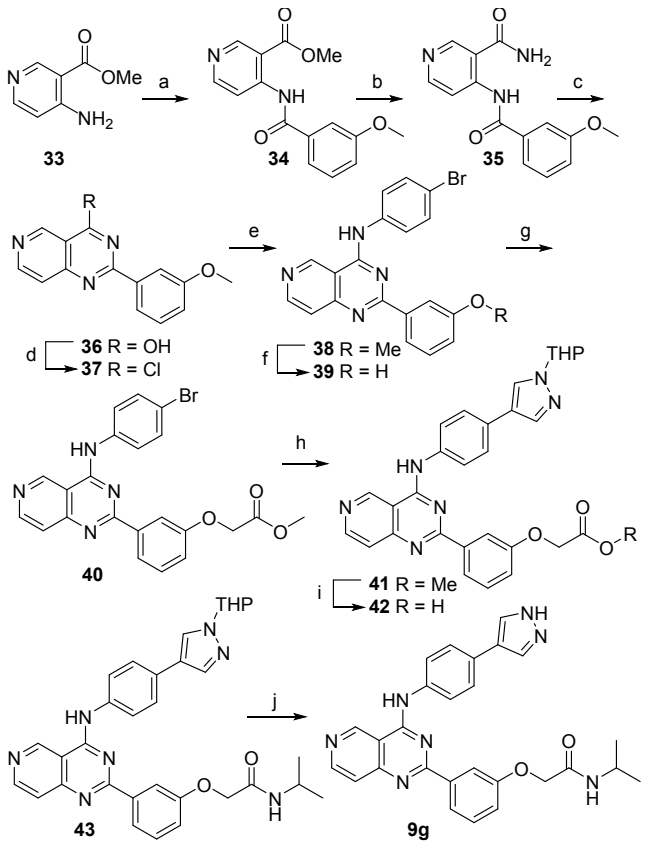

[a]Reagents and conditions: (a) 3-methoxybenzoyl chloride, TEA, DCM, rt, 16 h; (b) NH_3, MeOH, rt, 16 h; (c) NaOH, *i*PrOH, 90 °C, 3 h; (d) $POCl_3$, *i*Pr_2NEt, 80 °C, 14 h; (e) 4-bromoaniline, THF, 60 °C, 16 h; (f) BBr_3, 35 °C, 16 h; (g) methyl 2-bromoacetate, K_2CO_3, DMF, 40 °C, 1 h; (h) **24**, $Pd(dppf)Cl_2$, dioxane/water, 100 °C, 16 h; (i) LiOH, THF/water, 15 °C, 16 h; (j) HCl in dioxane, 15 °C, 1 h.

Scheme 4. General synthesis of tetrahydropyridopyrimidine derivatives[a]

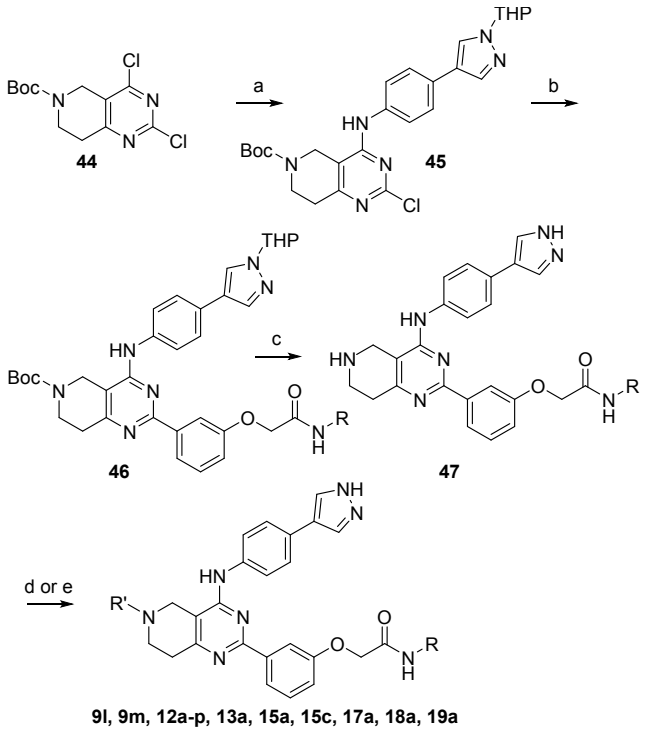

[a]Reagents and conditions: (a) **26**, *i*Pr_2NEt, *n*-BuOH, 100 °C, 16 h; (b) **23**, $Pd(dppf)Cl_2$, dioxane/water, 100 °C, 16 h; (c) HCl/dioxane/water, rt, 15 h; (d) aldehyde, $NaBH_3CN$, HOAc, MeOH, rt, 16 h; (e) R'Br, DMF, rt, 16 h.

Scheme 5. Second general synthesis of tetrahydropyridopyrimidine derivatives[a]

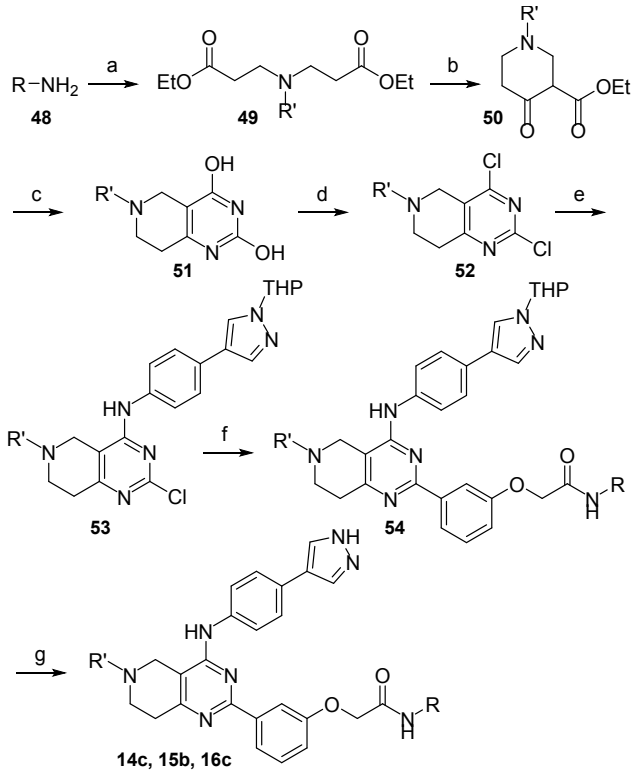

[a]Reagents and conditions: (a) ethyl acrylate, EtOH, rt, 72 h; (b) LiHMDS, THF, rt, 2 h; (c) Urea, NaOMe, MeOH, 80 °C, 16 h; (d) $POCl_3$, *i*Pr_2NEt, 90 °C, 16 h; (e) **26**, *i*Pr_2NEt, *n*-BuOH, 100 °C, 16 h; (f) **23**, $Pd(dppf)Cl_2$, dioxane/water, 100 °C, 16 h; (g) HCl/dioxane/water, rt, 15 h.

Both versions of the general synthesis depicted in Schemes 4 and 5 worked well to introduce variations in different regions of the molecule and were used to prepare gram quantities of material. However, these schemes are not ideal for the synthesis of large quantities of GLP or GMP grade material, due to some undesirable or low-yielding steps such as the Pd-mediated coupling and the reductive amination. For individual compounds, a more efficient synthesis was then developed. In Scheme 6, a scale-up synthesis of **15b** is presented, and it represents another general synthesis of this class of compounds. The key feature of this efficient convergent synthesis is that the amide moiety was pre-installed in amidine **58**, and the tetrahydropyridopyrimidine core was synthesized via a [3+3] cyclization. This robust synthesis allows less effort for purification of intermediates and has been used for greater than 100 g scales.

Scheme 6. Synthesis of **15b**[a]

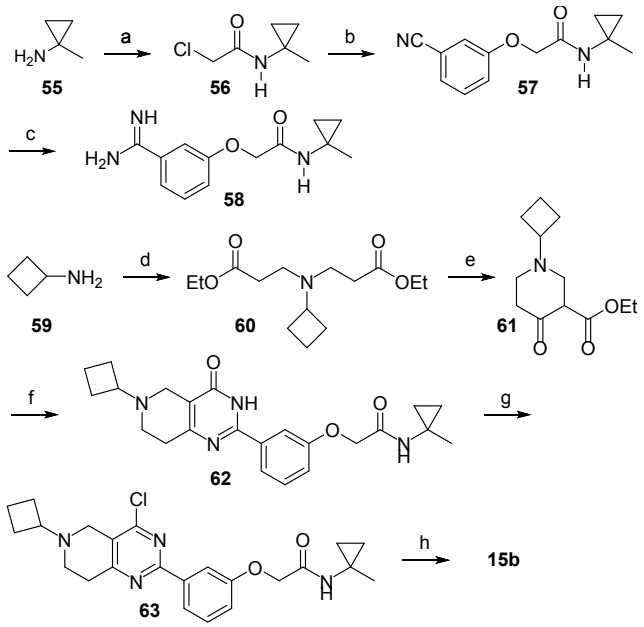

[a]Reagents and conditions: (a) 2-chloroacetyl chloride, TEA, DCM, -5 °C to 20 °C, 2 h, 72%; (b) 3-cyanophenol, K_2CO_3, CH_3CN, 10 °C to 80 °C, 24 h, 64%; (c) i. AcCl, EtOH, 0 °C to 20 °C, 12 h; ii. NH_3, EtOH, 20 °C to 25 °C, 11 h; (d) ethyl acrylate, EtOH, 20 °C, 72 h, 72%; (e) LiHMDS, THF, 20 °C, 2 h, 98%; (f) 58, NaOMe, 80 °C, 9 h, 60%; (g) $SOCl_2$, DMF, 0 °C to 20 °C, 9.5 h, 52%; (h) 4-(1*H*-pyrazol-4-yl)aniline, NMP, 145 °C, 5 h, 51%.

CONCLUSIONS

In summary, a class of potent and orally bioavailable inhibitors of glucose transport, targeting GLUT1/3, have been identified. SAR and optimization were carried out to improve the ADME, PK, and the brain penetration profile. Compound **15b** was identified with good GLUT1/3 potency, low brain penetration, and favorable ADME and PK profile across several different species and can serve as a valuable tool molecule to study GLUT functions *in vivo*.

EXPERIMENTAL SECTION

General. All solvents and reagents were obtained commercially and used as received. ^{1}H NMR spectra were recorded on a Bruker instrument (300 MHz, 400 MHz, or 500 MHz) in the cited deuterated solvents. Chemical shifts are given in ppm, and coupling constants are in hertz. All final compounds were purified by flash chromatography using 220-400 mesh silica gel or reverse-phase HPLC with CH_3CN/water as the solvents. Thin-layer chromatography was done on silica gel 60 F-254 (0.25-mm thickness) plates. Visualization was accomplished with UV light and/or 10% phosphomolybdic acid in ethanol. LC-MS experiments were done on a Shimadzu LCMS-2020 system. Compound purity was determined by a LC-MS or HPLC with 230 nm and 254 nm wavelengths. All final compounds reported here have purity ≥ 95%. All animal experiments performed in the manuscript were conducted in compliance with institutional guidelines. All efforts were made to minimize animal suffering, to reduce the number of animals.

Synthesis of 2-(3-(4-((4-(1H-Pyrazol-4-yl)phenyl)amino)-6-cyclobutyl-5,6,7,8-tetrahydropyrido[4,3-d]pyrimidin-2-yl)phenoxy)-N-(1-methylcyclopropyl)acetamide (**15b**)

Step 1. 2-Chloro-*N*-(1-methylcyclopropyl)acetamide (**56**).

To a mixture of 1-methylcyclopropan-1-amine hydrochloride **55** (200.0 g, 1.86 mol) and triethylamine (564.4 g, 5.58 mol) in DCM (1.0 L) was added 2-chloroacetyl chloride (220.6 g, 1.95 mol) drop-wise at -10 °C. The reaction mixture was then warmed to 20 °C and stirred at 20 °C for 12 h, poured into water, and washed with HCl (1.0 M, 4.0L). The combined organic layers were dried with anhydrous Na_2SO_4, filtered, and concentrated under vacuum to give the title compound (198.0 g, 72%) as a brown solid. ^{1}H NMR (400 MHz, DMSO-d_6) δ 8.42 (s, 1H), 3.93 (s, 2H), 1.27 (s, 3H), 0.62 – 0.53 (m, 4H). HRMS m/z calculated for $C_6H_{10}ClNO$ [M + H$^+$]: 148.0524, found 148.0529.

Step 2. *2-(3-Cyanophenoxy)-N-(1-methylcyclopropyl)acetamide (**57**).* To a mixture of 3-hydroxybenzonitrile (152.0 g, 1.28 mol) and K_2CO_3 (352.8 g, 2.55 mol) in CH_3CN (2.0 L) was added **56** (198.3 g, 1.34 mol) in portions. The mixture was stirred at 80 °C for 10 h, concentrated, and extracted with EtOAc (2.0 L × 3). The combined organic phases were dried with anhydrous Na_2SO_4, filtered, and concentrated to give a crude black solid. The crude product was triturated with EtOAc and MTBE/EtOAc to give the title compound as a brown solid (105 g). The mother liquor was concentrated and purified by chromatography to provide additional title compound (84.0 g). Total yield: 189 g, 64%. ^{1}H NMR (400 MHz, $CDCl_3$) δ 7.43 (m, 1H), 7.31 (m, 1H), 7.19 – 7.16 (m, 2H), 6.82 (s, 1H), 4.43 (s, 2H), 1.41 (s, 3H), 0.81 – 0.68 (m, 4H). HRMS m/z calculated for $C_{13}H_{14}N_2O_2$ [M + H$^+$]: 231.1128, found 231.1132.

Step 3. *2-(3-Carbamimidoylphenoxy)-N-(1-methylcyclopropyl)acetamide (**58**).* To a mixture of **57** (189.0 g, 0.821 mol) in EtOH (1.0 L) was added acetyl chloride (773.2 g, 9.85 mol) drop-wise at 0 °C. The mixture was stirred at 20 °C for 12 h and was concentrated and was then stirred with NH_3 in EtOH (2 L) for 10 h. The mixture was concentrated to provide a residue which was triturated with EtOH (300 mL) to afford the title compound (242.0 g) as a yellow solid. The crude material was used directly for in the next step reaction without further purification. ^{1}H NMR (400 MHz, DMSO-d_6) δ 9.33 (b, 3H), 8.46 (s, 1H), 7.53 (t, *J* = 8.0 Hz, 1H), 7.45-7.43 (m, 2H), 7.30-7.28 (m, 1H), 4.53 (s, 2H), 1.28 (s, 3H), 0.66-0.64 (m, 2H), 0.56-0.53 (m, 2H). HRMS m/z calculated for $C_{13}H_{17}N_3O_2$ [M + H+]: 248.1394, found 248.1395.

Step 4. Diethyl 3,3'-(cyclobutylazanediyl)dipropionate (**60**).

A mixture of cyclobutanamine **59** (300.0 g, 4.22 mol) and ethyl acrylate (1.24 kg, 12.39 mol) in EtOH (900 mL) was stirred at 30 °C for 72 h. The reaction mixture was concentrated under vacuum. The residual was purified by flash chromatography (SiO2, petroleum ether: ethyl acetate = 1:0 to 1:2) to give the title compound (823.0 g,

71.9%) as a yellow oil. ^{1}H NMR (400 MHz, $CDCl_3$) δ 4.03 (q, 4 H), 2.99 – 2.96 (m, 1 H) 2.66 (t, *J* = 7.2 Hz, 4 H), 2.32 (t, *J* = 7.6 Hz, 4 H), 1.95 – 1.91 (m, 2 H), 1.77 - 1.74 (m, 2 H), 1.53 - 1.48 (m, 2 H), 1.17 (t, *J* = 7.2 Hz, 6 H). HRMS m/z calculated for $C_{14}H_{25}NO_4$ [M + H$^+$]: 272.1856, found 272.1863.

Step 5. *Ethyl 1-cyclobutyl-4-oxopiperidine-3-carboxylate (**61**).* To LiHMDS in THF (1.0 M, 1.11 L) was added a solution of **60** (200.0 g, 0.727 mol) in THF (400 mL) under N2 atmosphere. The mixture was stirred at 20 °C for 2 h, quenched with saturated NH_4Cl (2.00 L), and extracted with ethyl acetate (2.00 L × 2). The combined organic phases were dried by Na_2SO_4 and concentrated *in vacuo* to provide the title compound (163.0 g, 98.2%) as a brown oil which was used directly in the next step reaction without further purification. ^{1}H NMR (400 MHz, DMSO-d_6) δ 4.21-4.09 (m, 2H), 3.53-3.50 (m, 1H), 2.90-2.69 (m, 4H), 2.48-2.30 (m, 3H), 2.00-1.98 (m, 2H), 1.83-1.77 (m, 2H), 1.65-1.61 (m, 2H), 1.24-1.17 (m, 3H). HRMS m/z calculated for $C_{12}H_{19}NO_3$ [M + H$^+$]: 226.1438, found 226.1437.

Step 6. *2-(3-(6-Cyclobutyl-4-oxo-3,4,5,6,7,8-hexahydropyrido[4,3-d]pyrimidin-2-yl)phenoxy)-N-(1-methylcyclopropyl)acetamide (**62**).* To a mixture of **61** (163.0 g, 0.724 mol) and **58** (119.3 g, 0.482 mol) in MeOH (1.6 L) was added NaOMe (104.2 g, 1.93 mol). The mixture was stirred at 80 °C for 9 h and was concentrated under a reduced pressure. The residual was diluted with H_2O (2.0 L) and neutralized with HCl. The mixture was filtrated and the cake was dried *in vacuo* to provide the title compound (118.7 g, 60.1%) as a yellow solid. ^{1}H NMR (400 MHz, DMSO-d_6) δ 12.58 (s, 1H), 8.33 (s, 1H), 7.68 (d, *J* = 8.0 Hz, 1H), 7.64 (s, 1H), 7.41 (t, *J* = 8.0, 1H), 7.14 (dd, *J* = 8.0, and 1.6 Hz, 1H), 4.47 (s, 2H), 3.16 (s, 2H), 2.89 - 2.70 (m, 1H), 2.66 - 2.64 (m, 2H), 2.55 - 2.54 (m, 2H), 2.06 - 2.05 (m, 2H), 1.86 - 1.83 (m, 2H), 1.69 - 1.67 (m, 2H), 1.29 (s, 3H), 0.67 – 0.64 (m, 2H), 0.64 – 0.55 (m, 2H). HRMS m/z calculated for $C_{23}H_{28}N_4O_3$ [M + H$^+$]: 409.2234, found 409.2250.

Step 7. *2-(3-(4-Chloro-6-cyclobutyl-5,6,7,8-tetrahydropyrido[4,3-d]pyrimidin-2-yl)phenoxy)-N-(1-methylcyclopropyl)acetamide (**63**).* A mixture of **62** (116.0 g, 0.284 mol) was dissolved in DMF (1.50 L) and was cooled to 0 °C. To the mixture was added $SOCl_2$ (50.7 g, 0.426 mol). The resulting mixture was stirred at 0 °C for 30 min followed by 20 °C for 9 h. The mixture was filtrated and the solid collected was washed with cold saturated sodium bicarbonate solution (1.0 L) and water. The solid was redissolved in dichloromethane, dried over Na_2SO_4, and concentrated *in vacuo* to afford the title compound (70.0 g, 57.7% yield) as a brown solid. ^{1}H NMR (400 MHz, $CDCl_3$) δ 8.07 (d, *J* = 8.4 Hz, 1H), 7.98 (d, *J* = 2.4 Hz, 1H), 7.40 (t, *J* = 8.0 Hz, 1H), 7.00 (dd, *J* = 8.4, 2.0 Hz, 1H), 6.91 (s, 1H), 4.51 (s, 2H), 3.53 (s, 2H), 3.07-3.02 (m, 3H), 2.73 (t, *J* = 6.0 Hz, 2H), 2.19-2.17 (m, 2H), 2.02-1.96 (m, 2H), 1.81-1.74 (m, 2H), 1.43 (s, 3H), 0.84-0.81 (m, 2H), 0.72-0.68 (m, 2H). HRMS m/z calculated for $C23H_{27}ClN_4O_2$ [M + H$^+$]: 427.1895, found 447.1897.

Step 8. 2-(3-(4-((4-(1H-Pyrazol-4-yl)phenyl)amino)-6-cyclobutyl-5,6,7,8-tetrahydropyrido[4,3-d]pyrimidin-2-yl)phenoxy)-N-(1-methylcyclopropyl)acetamide (**15b**). A mixture of **63** (145.0 g, 0.340 mol), 4-(1H-pyrazol-4-yl)aniline (54.1 g, 0.340 mol), and N-methyl-2-pyrrolidone (580 mL) was stirred at 145 °C for 5 h, diluted with CH_3CN (1.50 L), and filtered. The filter cake was dissolved with Conc. HCl (500 ml) and MeOH (3 L). The resulting solution was concentrated to give a crude material which was purified by prep-HPLC to give the title compound as a yellow HCl salt solid (102.2 g, 51.4%). ^{1}H NMR (400 MHz, CD_3OD) δ 8.12 (s, 2H), 7.88 (d, J = 8.0 Hz, 1H), 7.83 (m, 1H), 7.73 (m, 4H), 7.49 (t, J = 8.0 Hz, 1H), 7.26 (dd, J = 8.0,and 2.0 Hz, 1H), 4.52 (s, 2H), 4.38 (s, 2H), 4.08 - 3.99 (m, 1H), 3.64 (s, 2H), 3.36 (t, J = 5.2 Hz, 2H), 2.54- 2.50 (m, 4H), 2.02 - 1.95 (m, 2H), 1.35 (s, 3H), 0.72 (m, 2H), 0.62 (m, 2H); ^{13}C NMR (101 MHz, DMSO-d_6) δ 168.24, 159.75, 158.39, 157.19, 156.52, 137.15, 136.65, 131.10, 130.20, 129.36, 125.61, 123.64, 121.41, 121.22, 118.38, 114.33, 105.66, 67.42, 58.56, 45.05, 44.47, 28.63, 27.23, 25.40, 25.35, 23.03, 14.01. HRMS m/z calculated for $C_{32}H_{36}N_7O_2$ [M + H$^+$]: 550.2925, found 550.2912.

GLUT, GLUT1 and GLUT3 assays

GLUT1 and GLUT3 assays were performed using a modified version of the pairwise assay described by Siebeneicher et al.[22]. Briefly, GLUT1-dependent DLD1 wild-type and GLUT3-dependent DLD1-*SLC2A1*$^{-/-}$ (Horizon Discovery) were maintained in RPMI 1640 cell culture medium containing 10% fetal bovine serum, 1% penicillin-streptomycin and 10 mM HEPES in a humidified incubator with 5% CO_2 at 37° C. The day before the assay, the cells were seeded in 90 µL of this medium in 96-well plates at a density of 50,000 cells/well and allowed to attach overnight. The day of the assay, 10 µL of culture medium containing GLUT inhibitors and oligomycin was added to each well to a final concentration of 10 µM oligomycin and 0.06% DMSO. The plates were returned to the incubator for 90 minutes and then ATP levels were determined using the CellTiter-Glo® Luminescent Cell Viability Assay (Promega). For GLUT HT-1080 assay, the procedure was the same except the cells were seeded at 40,000 cells/well.

Glucose competition assay

The assay was performed according to the standard GLUT1 (DLD-1) assay protocol, except that the cells were washed once in 100 µL PBS prior to addition of media containing the test compounds, oligomycin (10 µM) and the glucose at either 10, 3.33, 1.11 or 0.37 mM concentration.

ASSOCIATED CONTENT

Supporting Information

The Supporting Information is available free of charge on the ACS Publications website at DOI: xxx.

Details of the synthetic procedures and analytical data for intermediates and final compounds **9a-m, 10a-i, 11a, 11b, 12a-p, 13a, 14b, 14c, 15a, 15c, 16c, 17a, 18a, 19a** (S1-S46); Table S1. GLUT1 IC_{50} values (nM) in the presence of varying glucose concentrations (S47); Table S2. Eurofins safety panel screen of **15b** (S48).

Molecular formula strings are available separately in comma-separated values file format (CSV).

AUTHOR INFORMATION

Corresponding Author

*K.G.L.: e-mail, kevin.liu@kadmon.com.

ACKNOLEDGMENT

The authors thank Professor Joshua D. Rabinowitz of Princeton University for his valuable insights and suggestions and Yong Li, Yafeng Cao, Binglin Wang, Xian Xiao, and others involved at WuXi AppTec (Wuhan) for their synthetic support.

ABBREVIATIONS USED

ADME, adsorption, distribution, metabolism, and excretion; Ac, acetyl; AUC, area under the curve; BCRP, breast cancer resistance protein; BBB, blood-brain barrier; CNS, central nervous system; CL, clearance; Da, Dalton; DCM, dichloromethane; DHP, 3,4-dihydropyran; DMAP, 4-(dimethylamino)pyridine; DMF, N,N-dimethylformamide; GLUT, glucose transporters; IC50, inhibitory concentration at half maximal effect; 18F-FDG, [18F]fluoro-2-deoxyglucose; fu, unbound fraction; iv, intravenous; LM, liver microsomes; LiHMDS, lithium bis(trimethylsilyl)amide; mM, millimolar; μM, micromolar; OXPHOS, oxidative phosphorylation; P-gp, P-glycoprotein; Pd(dppf)Cl2, [1,1□-bis(diphenylphosphino)ferrocene]dichloropalladium(II); PK, pharmacokinetic; po, oral administration; RO5, rule of five (Lipinski); SAR, structure–activity relationship; TCA, tricarboxylic acid; Th, T helper; THP, 2-tetrahydropyranyl; *p*-TsOH, *p*-Toluenesulfonic acid; Vdss, volume of distribution at steady state.

REFERENCES

1. Warburg, O. U¨Ber Den Stoffwechsel Der Carcinomzelle. *Naturwissenschaften* **1924**, *12*, 1131-1137.
2. Warburg, O. On the Origin of Cancer Cells. *Science* **1956**, *123*, 309-314.
3. Altenberg, B.; Greulich, K. O. Genes of Glycolysis Are Ubiquitously Overexpressed in 24 Cancer Classes. *Genomics* **2004**, *84*, 1014-1020.
4. Upadhyay, M.; Samal, J.; Kandpal, M.; Singh, O. V.; Vivekanandan, P. The Warburg Effect: Insights from the Past Decade. *Pharmacol. Ther.* **2013**, *137*, 318-330.
5. DeBerardinis, R. J.; Lum, J. J.; Hatzivassiliou, G.; Thompson, C. B. The Biology of Cancer: Metabolic Reprogramming Fuels Cell Growth and Proliferation. *Cell Metab.* **2008**, *7*, 11-20.
6. Vander Heiden, M. G.; Cantley, L. C.; Thompson, C. B. Understanding the Warburg Effect: The Metabolic Requirements of Cell Proliferation. *Science* **2009**, *324*, 1029-1033.
7. Pearce, E. L.; Poffenberger, M. C.; Chang, C.-H.; Jones, R. G. Fueling Immunity: Insights into Metabolism and Lymphocyte Function. *Science* **2013**, *342*, 1242454.
8. Hotamisligil, G. S. Foundations of Immunometabolism and Implications for Metabolic Health and Disease. *Immunity* **2017**, *47*, 406-420.
9. Palmer, C. S.; Ostrowski, M.; Balderson, B.; Christian, N.; Crowe, S. M. Glucose Metabolism Regulates T Cell Activation, Differentiation, and Functions. *Front. Immunol.* **2015**, *6*, 1-6.
10. Macintyre, A. N.; Gerriets, V. A.; Nichols, A. G.; Michalek, R. D.; Rudolph, M. C.; Deoliveira, D.; Anderson, S. M.; Abel, E. D.; Chen, B. J.; Hale, L. P.; Rathmell, J. C. The Glucose Transporter Glut1 Is Selectively Essential for Cd4 T Cell Activation and Effector Function. *Cell Metab.* **2014**, *20*, 61-72.
11. Navale, A. M.; Paranjape, A. N. Glucose Transporters: Physiological and Pathological Roles. *Biophys. Rev.* **2016**, *8*, 5-9.
12. Deng, D.; Xu, C.; Sun, P.; Wu, J.; Yan, C.; Hu, M.; Yan, N. Crystal Structure of the Human Glucose Transporter Glut1. *Nature* **2014**, *510*, 121-125.
13. Deng, D.; Sun, P.; Yan, C.; Ke, M.; Jiang, X.; Xiong, L.; Ren, W.; Hirata, K.; Yamamoto, M.; Fan, S.; Yan, N. Molecular Basis of Ligand Recognition and Transport by Glucose Transporters. *Nature* **2015**, *526*, 391-396.
14. Adekola, K.; Rosen, S. T.; Shanmugam, M. Glucose Transporters in Cancer Metabolism. *Curr. Opin. Oncol.* **2012**, *24*, 650-654.
15. Granchi, C.; Fancelli, D.; Minutolo, F. An Update on Therapeutic Opportunities Offered by Cancer Glycolytic Metabolism. *Bioorg. Med. Chem. Lett.* **2014**, *24*, 4915-4925.
16. Barron, C. C.; Bilan, P. J.; Tsakiridis, T.; Tsiani, E. Facilitative Glucose Transporters: Implications for Cancer Detection, Prognosis and Treatment. *Metabolism* **2016**, *65*, 124-139.
17. Liu, Y.; Cao, Y.; Zhang, W.; Bergmeier, S.; Qian, Y.; Akbar, H.; Colvin, R.; Ding, J.; Tong, L.; Wu, S.; Hines, J.; Chen, X. A Small-Molecule Inhibitor of Glucose Transporter 1 Downregulates Glycolysis, Induces Cell-Cycle Arrest, and Inhibits Cancer Cell Growth in Vitro and in Vivo. *Mol. Cancer Ther.* **2012**, *11*, 1672-1682.
18. Wang, D.; Chu, P. C.; Yang, C. N.; Yan, R.; Chuang, Y. C.; Kulp, S. K.; Chen, C. S. Development of a Novel Class of Glucose Transporter Inhibitors. *J. Med. Chem.* **2012**, *55*, 3827-3836.
19. Chan, D. A.; Sutphin, P. D.; Nguyen, P.; Turcotte, S.; Lai, E. W.; Banh, A.; Reynolds, G. E.; Chi, J. T.; Wu, J.; Solow-Cordero, D. E.; Bonnet, M.; Flanagan, J. U.; Bouley, D. M.; Graves, E. E.; Denny, W. A.; Hay, M. P.; Giaccia, A. J. Targeting Glut1 and the Warburg Effect in Renal Cell Carcinoma by Chemical Synthetic Lethality. *Sci. Transl. Med.* **2011**, *3*, 94ra70.
20. Kapoor, K.; Finer-Moore, J. S.; Pedersen, B. P.; Caboni, L.; Waight, A.; Hillig, R. C.; Bringmann, P.; Heisler, I.; Muller, T.; Siebeneicher, H.; Stroud, R. M.

Mechanism of Inhibition of Human Glucose Transporter Glut1 Is Conserved between Cytochalasin B and Phenylalanine Amides. *Proc. Natl. Acad. Sci. U. S. A.* **2016**, *113*, 4711-4716.

21. Siebeneicher, H.; Bauser, M.; Buchmann, B.; Heisler, I.; Muller, T.; Neuhaus, R.; Rehwinkel, H.; Telser, J.; Zorn, L. Identification of Novel Glut Inhibitors. *Bioorg. Med. Chem. Lett*. **2016**, *26*, 1732-1737.
22. Siebeneicher, H.; Cleve, A.; Rehwinkel, H.; Neuhaus, R.; Heisler, I.; Muller, T.; Bauser, M.; Buchmann, B. Identification and Optimization of the First Highly Selective Glut1 Inhibitor Bay-876. *ChemMedChem* **2016**, *11*, 2261-2271.
23. Reckzeh, E. S.; Karageorgis, G.; Schwalfenberg, M.; Ceballos, J.; Nowacki, J.; Stroet, M. C. M.; Binici, A.; Knauer, L.; Brand, S.; Choidas, A.; Strohmann, C.; Ziegler, S.; Waldmann, H. Inhibition of Glucose Transporters and Glutaminase Synergistically Impairs Tumor Cell Growth. *Cell. Chem. Biol*. **2019**, *26*, 1214-1228 e1225.
24. Sergeant, S.; Kim, H. D. Inhibition of 3-O-Methylglucose Transport in Human Erythrocytes by Forskolin. *J. Biol. Chem*. **1985**, *260*, 14677-14682.
25. Ritchie, T. J.; Macdonald, S. J. The Impact of Aromatic Ring Count on Compound Developability--Are Too Many Aromatic Rings a Liability in Drug Design? *Drug Discov. Today* **2009**, *14*, 1011-1020.
26. Lovering, F.; Bikker, J.; Humblet, C. Escape from Flatland: Increasing Saturation as an Approach to Improving Clinical Success. *J. Med. Chem*. **2009**, *52*, 6752-6756.
27. Lipinski, C. A.; Lombardo, F.; Dominy, B. W.; Feeney, P. J. Experimental and Computational Approaches to Estimate Solubility and Permeability in Drug Discovery and Development Settings. Adv. Drug. *Deliv. Rev*. **2001**, *46*, 3-26.
28. Hitchcock, S. A.; Pennington, L. D. Structure-Brain Exposure Relationships. *J. Med. Chem*. **2006**, *49*, 7559-7583.
29. Wager, T. T.; Hou, X.; Verhoest, P. R.; Villalobos, A. Moving Beyond Rules: The Development of a Central Nervous System Multiparameter Optimization (cns mpo) Approach to Enable Alignment of Druglike Properties. *ACS Chem. Neurosci*. **2010**, *1*, 435-449.
30. Ghose, A. K.; Herbertz, T.; Hudkins, R. L.; Dorsey, B. D.; Mallamo, J. P. Knowledge-Based, Central Nervous System (Cns) Lead Selection and Lead Optimization for Cns Drug Discovery. *ACS Chem. Neurosci.* **2012**, *3*, 50-68.
31. Rankovic, Z. Cns Physicochemical Property Space Shaped by a Diverse Set of Molecules with Experimentally Determined Exposure in the Mouse Brain. *J. Med. Chem*. **2017**, *60*, 5943-5954.
32. Palm, K.; Luthman, K.; Ros, J.; Grasjo, J.; Artursson, P. Effect of Molecular Charge on Intestinal Epithelial Drug Transport: Ph-Dependent Transport of Cationic Drugs. *J. Pharmacol. Exp. Ther*. **1999**, *291*, 435-443.
33. Gillis, E. P.; Eastman, K. J.; Hill, M. D.; Donnelly, D. J.; Meanwell, N. A. Applications of Fluorine in Medicinal Chemistry. *J. Med. Chem*. **2015**, *58*, 8315-8359.
34. Meanwell, N. A. Fluorine and Fluorinated Motifs in the Design and Application of Bioisosteres for Drug Design. *J. Med. Chem*. **2018**, *61*, 5822-5880.
35. Sugano, K.; Kansy, M.; Artursson, P.; Avdeef, A.; Bendels, S.; Di, L.; Ecker, G. F.; Faller, B.; Fischer, H.; Gerebtzoff, G.; Lennernaes, H.; Senner, F. Coexistence of Passive and Carrier-Mediated Processes in Drug Transport. *Nat. Rev. Drug. Discov*. **2010**, *9*, 597-614.
36. Bagal, S.; Bungay, P. Restricting Cns Penetration of Drugs to Minimise Adverse Events: Role of Drug Transporters. *Drug Discov. Today Technol*. **2014**, *12*, e79-85.
37. Volpe, D. A. Drug-Permeability and Transporter Assays in Caco-2 and Mdck Cell Lines. *Future Med. Chem*. **2011**, *3*, 2063-2077.
38. Olszewski, K.; Kim, J.-I.; Poyurovsky, M.; Liu, K.; Barsotti, A.; Morris, K. Preparation of Fused Pyrimidines as Glucose Uptake Inhibitors. WO2016210330A1, 2016.

Table of Contents graphic

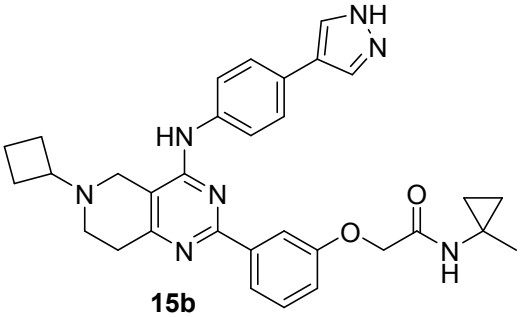

15b

GLUT1 IC_{50} = 242 nM
GLUT3 IC_{50} = 179 nM
Oral *F* = 45.5% (mouse) and 49.4% (rat)